



Side-reaction products identified for photo-nuclear production of ^{99}Mo

Peter Tkac¹ · Sergey Chemerisov² · Roman Gromov² · Jeongseog Song³ · Jerry Nolen³ · Vakhtang Makarashvili⁴ · George Vandegrift¹

Received: 7 May 2020 / Published online: 13 August 2020

© This is a U.S. Government work and not under copyright protection in the US; foreign copyright protection may apply 2020

Abstract

Production of ^{99}Mo by the $^{100}\text{Mo}(\gamma, n)^{99}\text{Mo}$ reaction through the bremsstrahlung process using an electron accelerator is one of the feasible options currently pursued by several countries. Here we report experimental results on identification of side-reaction products after the irradiation of natural and enriched ^{100}Mo targets. Side-reaction products identified include various Mo, Nb and Zr isotopes. Comparison of experimentally determined reaction production rates with those determined based on theoretical cross-sections will be presented. Moreover, activation products formed due to presence of impurities introduced during the manufacturing of the Mo targets will also be discussed.

Keywords Molybdenum · Mo-99 · Accelerator production · Side-reaction products · Monte Carlo

Introduction

The most-used medical isotope for imaging, technetium- $^{99\text{m}}$, the daughter of ^{99}Mo , is currently produced by fission of ^{235}U in nuclear reactors because of the very high fission yield (6.1%) and the high thermal neutron fission cross section [1]. Most of the reactors used for the production of ^{99}Mo have been operating for decades. Recently, one of the major suppliers of ^{99}Mo , Nordion (Canada) ended processing of irradiated targets for production of ^{99}Mo , since the Chalk River reactor in Canada ceased its operation due to the age of the reactor. Many countries are looking for alternative production pathways for ^{99}Mo because of the regulatory approvals required for fission-made molybdenum and the complicated and expensive waste disposal options. Although neutron capture in a reactor using enriched ^{98}Mo targets by the $^{98}\text{Mo}(n, \gamma)^{99}\text{Mo}$ reaction can be used, the process still relies on the availability of a research or commercial reactor.

Accelerator technology provides a valuable alternative: The direct production of $^{99\text{m}}\text{Tc}$ using the $^{100}\text{Mo}(p, 2n)^{99\text{m}}\text{Tc}$ reaction by cyclotrons [2–6] can be adopted by countries that have an infrastructure of strategically placed cyclotrons currently being used for the production of other medical isotopes, such as ^{18}F . In addition, electron-beam accelerators can be used for production of ^{99}Mo through the bremsstrahlung process via the $^{100}\text{Mo}(\gamma, n)^{99}\text{Mo}$ reaction [7–10]. This is a very strong alternative because of the commercial availability of these accelerators, an easier waste disposal pathway, and the potential for producing kilocurie (kCi, $1\text{ kCi} = 37\text{ GBq}$) quantities of ^{99}Mo . For kCi quantities of ^{99}Mo , several-hundred-gram targets consisting of enriched ^{100}Mo are required, and, due to the high cost of enriched ^{100}Mo material, efficient recycling processes need to be in place. Recently, several studies of enriched Mo recycling [3, 11–14] reported recovery yields ranging from ~85 to ~98%.

Argonne National Laboratory, with support from the National Nuclear Security Administration's Office of Material Management and Minimization, is providing technical development assistance to NorthStar Medical Technologies, LLC in its pursuit of ^{99}Mo production without the use of highly-enriched uranium. The U.S. Food and Drug Administration recently approved NorthStar's RadioGenix® system for producing sodium pertechnetate from a low-specific-activity ^{99}Mo solution [15]. NorthStar is currently producing ^{99}Mo via a $^{98}\text{Mo}(n, \gamma)^{99}\text{Mo}$ reaction (neutron capture) pathway at the University of Missouri Research Reactor

✉ Peter Tkac
tkac@anl.gov

¹ Chemical and Fuel Cycle Technologies Division, 9700 S. Cass Ave, Lemont, IL 60439, USA

² Experimental Operations and Facilities Division, 9700 S. Cass Ave, Lemont, IL 60439, USA

³ Physics Division, 9700 S. Cass Ave, Lemont, IL 60439, USA

⁴ Argonne National Laboratory, 9700 S. Cass Ave, Lemont, IL 60439, USA

Center. Soon, a second production option will be available: the photonuclear reaction $^{100}\text{Mo}(\gamma, n)^{99}\text{Mo}$ from irradiation of enriched Mo targets by an electron accelerator. Although there are several reports discussing Mo cross sections [16, 17] and the formation of side-reaction products during the photonuclear reaction on ^{100}Mo targets [18, 19] most are based on theoretical cross sections or very short irradiation [20, 21]. Identification of the production rates for side-reaction products formed during the accelerator production of ^{99}Mo provides a better understanding of how the isotopic composition of the Mo target and the presence of other impurities can affect the final purity of the ^{99}Mo product. This is particularly important for tracking the level of certain impurities or when considering whether to use natural or isotopically ^{100}Mo enriched targets, due to long half-lives and a potential build-up of activity.

Here we report experimental data on side-reaction product yields collected after 0.5 and 4 h irradiations of natural ultra-high-purity (UHP) Mo and ^{100}Mo -enriched disks (both provided by NorthStar). Experimentally determined production rates are also compared to theoretically estimated production rates based on the JENDL photonuclear reaction cross section database and the particle and heavy ion transport-code system PHITS 3.02 simulation tool.

Experimental

Linac irradiations

Argonne's low-energy and high-power electron linac was used as the source of the electron beam for the experiments. This electron linac operates with repetition rates

up to 240 Hz with maximum beam power of up to 110 W per pulse. Effective beam energy is in the range of 20 to 50 MeV. The highest beam energy is about 53 MeV. The DC thermal gun produces electron beam pulses with amplitude up to 2.0 A and length up to 5.5 μs . RF power for the two accelerating structures is provided by two Thales TV2022A klystrons. After acceleration, the beam goes through an evacuated transport channel to the experimental hall and is delivered to the target face. Steering coils and quadrupole magnets keep the beam in the proper shape and position [22].

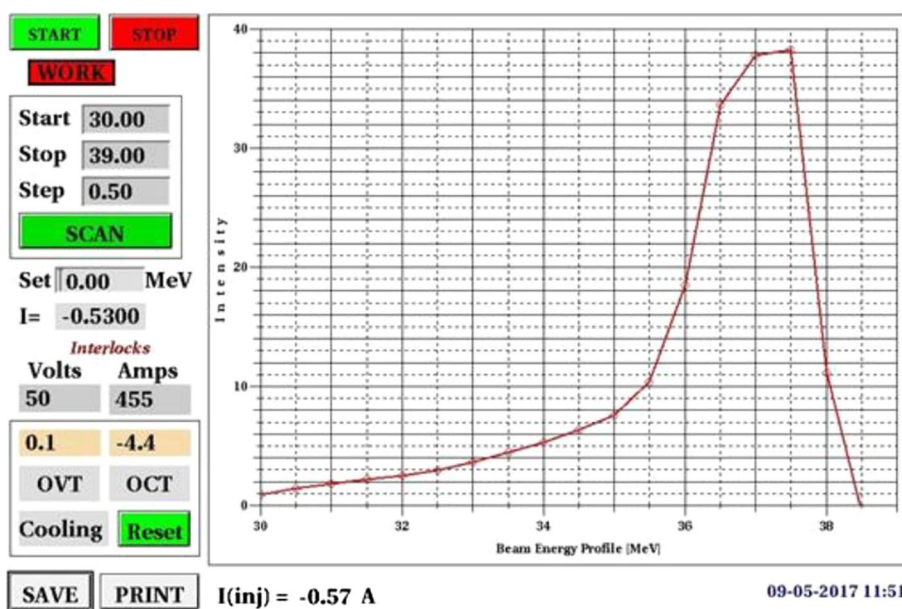
Mo irradiation runs were performed with a 40 MeV electron beam energy and beam parameters presented in Table 1. The typical beam energy spectrum at 37 MeV is shown in Fig. 1. The energy spectrum width was about ± 0.9 MeV or $\pm 2.3\%$ at half of the maximum amplitude. The transverse beam shape at the converter was elliptical, with a width of 5 mm and a height of 3 mm full width at half maximum (FWHM). The accelerated beam pulse current for the 40 MeV beam energy was about 0.49 A.

The cooling water flow through the converter was 11.3 L/min (3 gpm). To control the temperature of the window, two 1/16-inch thermocouples were installed at the tested window holder.

Table 1 Irradiation conditions and times for natural ultra-high purity (UHP) and ^{100}Mo -enriched Mo targets

MeV	Irradiation time (h)	Power (kW)	Target mass (g)	
			UHP Mo	Enriched ^{100}Mo
40	4	1.5	0.9719	0.4294
40	0.5	1.5	0.9736	0.6254

Fig. 1 Typical beam energy spectrum produced by Argonne's electron linac and the load lines



Monte Carlo calculations

In order to estimate production rates for all isotopes produced by the photonuclear reaction in the entire target system, simulations were done using the Monte Carlo simulation code PHITS 3.02. The major improvements to the photonuclear yield calculation in the latest version of PHITS include (1) replacement of the total reaction cross sections in the Japanese Evaluated Nuclear Data Library (JENDL/PD 2004), which contains measured data for 68 nuclei, (2) modification of the evaporation model for the giant resonance, and (3) implementation of the quasideuteron disintegration process. These improvements allow PHITS to examine a photonuclear reaction up to 140 MeV of incident photon energy and cover our bremsstrahlung photon energy range of 0–40 MeV. A new parameter was added to reflect the contribution of nucleus recoil from elastic scattering in the yield calculation. When comparing the production rates of simulations and experiments, simulations excluding elastic collision produce predictions that significantly underestimate weak channels such as $(\gamma, x + n)$, $(\gamma, p + n)$, and isomeric states. However, simulation predictions including elastic collision are quite close to the experiments, without any change in production rates for well-known strong channels such as (γ, n) . Elastic collision may have been an important factor in the prediction of production rates for weak channels; therefore, we performed the simulations including elastic collision.

Geometry

For Monte Carlo simulations, we used an incident electron beam with a beam power of 1.5 kW at 40 MeV, assuming a FWHM beam size of 1 cm in a Gaussian shape. To produce the bremsstrahlung photons, the beam impinged on a water-cooled convertor consisting of six 0.5-mm-thick tantalum disks. The Mo targets were positioned on the right, and the beam struck from the left (Fig. 2). Dimensions of 1 mm thick and 12.7 mm in diameter were used for both the natural and enriched ^{100}Mo targets in the simulations. Enriched targets were split into two pieces: one portion was used for the 0.5 h irradiation and the second for the 4 h irradiation (Table 1). Natural and enriched ^{100}Mo targets were irradiated together.

X-ray flux and its energy distribution

The calculated (PHITS) bremsstrahlung photon fluxes generated by interactions with the convertors before the Mo targets are shown in Fig. 3. The photon beam flux vs. its energy as the target's radius changes is shown in the left panel, and beam flux as a function of radius was plotted in the right panel. In this simulation, the radii of the targets were extended to 1.6 cm to determine the detailed beam

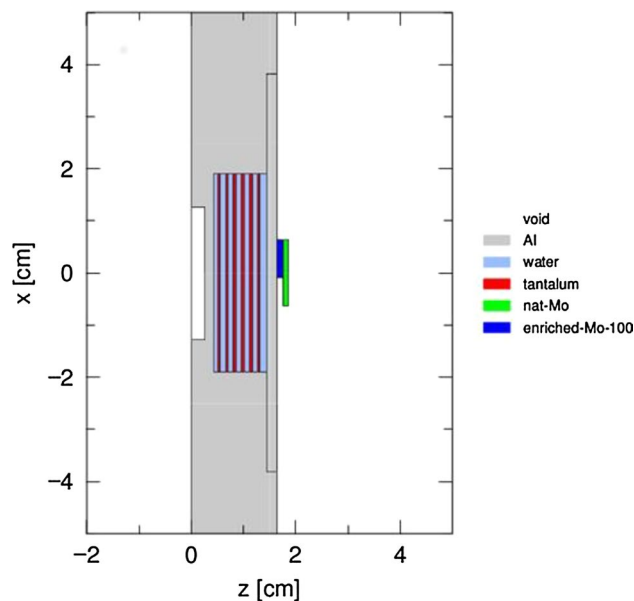


Fig. 2 Geometry of clamshell setup for natural and enriched ^{100}Mo targets

flux dependence by radius. The beam flux at the edge of our target (6 mm in radius) decreased by about 50% compared to that at the center. These simulations can be used to increase the production yield by adjusting the diameter and thickness of the Mo target when the target mass is fixed for the production run.

Irradiated Mo targets

Natural isotopic composition Mo targets (^{92}Mo —14.84%, ^{94}Mo —9.25%, ^{95}Mo —15.92%, ^{96}Mo —16.68%, ^{97}Mo —9.55%, ^{98}Mo —24.13%, ^{100}Mo —9.63%) were made from ultra-high-purity (UHP) MoO_3 that was converted to Mo metal powder and pressed and sintered into 12×1 mm Mo disks. Elemental analysis of UHP Mo material for 77 elements showed only appreciable amounts of Ni (0.3 ppm), Cu (0.5 ppm), Zr (0.14 ppm), Sn (0.03 ppm), Sb (1 ppm), Cs (0.1 ppm), and U (0.06 ppm); other elements were below the detection limit. The disks were provided by NorthStar. In a similar way, NorthStar provided ^{100}Mo -enriched targets (97.39% ^{100}Mo content, 2.59% ^{98}Mo ; the presence of other Mo isotopes was not reported). The major impurities identified in the enriched ^{100}Mo targets were as follow: Fe (540 ppm), Cr (64 ppm), W (75.1 ppm), Ni (39.4 ppm), Cu (14.9 ppm), Ge (11.4 ppm), and Mn (5.7 ppm). One UHP natural Mo and one ^{100}Mo -enriched target were placed together and wrapped in aluminum foil. Each target was then mounted in aluminum target holder for irradiation. Targets were mounted right on the surface of the tantalum water-cooled converter. Tantalum was chosen for its high Z value,

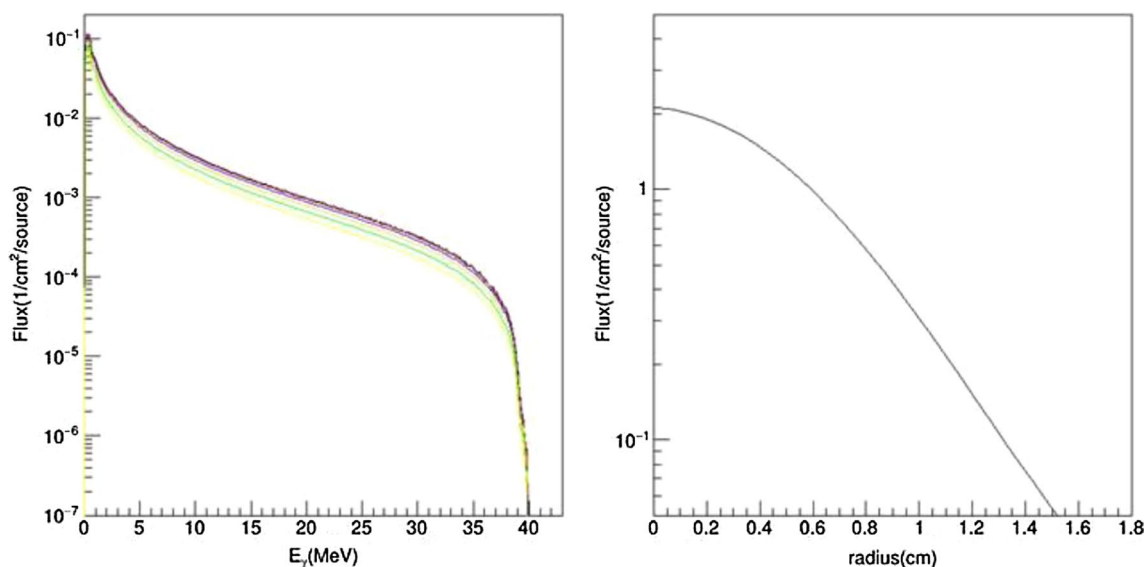


Fig. 3 Left: flux vs. energy from 0.5 mm (black—on top) to 6 mm (yellow) in radius. Right: radial dependence of photon flux in the Mo target

high melting point, chemical stability, and good machinability. A schematic of the irradiation setup can be seen in Fig. 2.

Gamma counting of irradiated Mo targets

Short (0.5 h) irradiations were used to identify short-lived isotopes. The short irradiation time allowed for the retrieval of the irradiated targets right after irradiation, and for gamma counting within an hour of the end of bombardment (EOB). Longer-lived isotopes were counted after some delay

to allow for the decay of short-lived isotopes and to decrease the dead time on the HPGe detector. Each irradiated target was counted more than three times at different times to confirm that the selected peak does not interfere with different gamma lines. This was confirmed by the decay correction to EOB. Major radionuclides identified together with their production pathway, major gamma peak, and half-life are listed in Table 2. Theoretical cross sections for photonuclear reactions listed in Table 2 could be found online at TENDL database. HPGe gamma detector was calibrated

Table 2 Major radionuclides identified after irradiation of natural and ^{100}Mo enriched targets, their production pathway, main gamma energy peak and half-life (obtained from Nuclide Navigator, Ortec)

Nuclide	Potential production pathway	Main energy peak (keV)	Half-life (h)
^{90}Mo	$^{92}\text{Mo}(\gamma, 2n)^{90}\text{Mo}$	257.34	5.67
$^{93\text{m}}\text{Mo}$	$^{94}\text{Mo}(\gamma, n)^{93\text{m}}\text{Mo}$ $^{95}\text{Mo}(\gamma, 2n)^{93\text{m}}\text{Mo}$ $^{96}\text{Mo}(\gamma, 3n)^{93\text{m}}\text{Mo}$	1477.2	6.95
^{99}Mo	$^{100}\text{Mo}(\gamma, n)^{99}\text{Mo}$	739.5	66.19
$^{91\text{m}}\text{Nb}$	$^{92}\text{Mo}(\gamma, p)^{91\text{m}}\text{Nb}$ $^{94}\text{Mo}(\gamma, 2n + p)^{91\text{m}}\text{Nb}$	1205	1536.12
$^{92\text{m}}\text{Nb}$	$^{94}\text{Mo}(\gamma, p + n)^{92\text{m}}\text{Nb}$ $^{95}\text{Mo}(\gamma, 2n + p)^{92\text{m}}\text{Nb}$	934.5	243.84
$^{95\text{m}}\text{Nb}$	$^{96}\text{Mo}(\gamma, p)^{95\text{m}}\text{Nb}$ $^{97}\text{Mo}(\gamma, p + n)^{95\text{m}}\text{Nb}$ $^{98}\text{Mo}(\gamma, 2n + p)^{95\text{m}}\text{Nb}$	235.4	86.592
^{95}Nb	$^{96}\text{Mo}(\gamma, p)^{95}\text{Nb}$ $^{97}\text{Mo}(\gamma, p + n)^{95}\text{Nb}$ $^{98}\text{Mo}(\gamma, 2n + p)^{95}\text{Nb}$	765.8	839.52
^{96}Nb	$^{97}\text{Mo}(\gamma, p)^{96}\text{Nb}$ $^{98}\text{Mo}(\gamma, p + n)^{96}\text{Nb}$	1091.5	23.35
^{97}Nb	$^{98}\text{Mo}(\gamma, p)^{97\text{m}}\text{Nb}$ $^{100}\text{Mo}(\gamma, 2n + p)^{97}\text{Nb}$	657.9	1.233
$^{98\text{m}}\text{Nb}$	$^{100}\text{Mo}(\gamma, p + n)^{98\text{m}}\text{Nb}$	787.2	0.852
^{88}Zr	$^{92}\text{Mo}(\gamma, \alpha)^{88}\text{Zr}$	392.85	2001.6
^{88}Y	$^{88}\text{Zr} \rightarrow ^{88}\text{Y}$	1836 & 898	2558.4
^{95}Zr	$^{97}\text{Mo}(\gamma, 2p)^{95}\text{Zr}$ $^{98}\text{Mo}(\gamma, n + 2p)^{95}\text{Zr}$ $^{100}\text{Mo}(\gamma, n + \alpha)^{95}\text{Zr}$	724.18	1536.48
^{54}Mn	impurity $^{55}\text{Mn}(\gamma, n)^{54}\text{Mn}$	834.8	7490.4
^{51}Cr	impurity $^{52}\text{Cr}(\gamma, n)^{51}\text{Cr}$	320.07	664.8
^{57}Co	impurity $^{58}\text{Ni}(\gamma, p)^{57}\text{Co}$	122.1	6480

using multi-nuclide gamma standard (Eckert & Ziegler) and spectra were analyzed using GammaVision software (Ortec). The detector had appropriate energy and efficiency calibration obtained using multi-nuclide standard at each distance used for gamma counting of the samples. Decay correction during acquisition was used to account for decay of radionuclides during longer count times. Whole irradiated Mo disks and fractures (in case of ^{100}Mo enriched material) were counted facing the detector in flat orientation at various distances up to 2 m from the detector.

Due to ingrowth of ^{95}Nb from $^{95\text{m}}\text{Nb}$ and ^{95}Zr , ^{95}Nb activity at EOB was calculated as follows:

$$A_{\text{Nb95}}^0 = \frac{A_{\text{Nb95}} - \frac{\lambda_{\text{Nb95}} A_{\text{Nb95m}}^0}{\lambda_{\text{Nb95}} - \lambda_{\text{Nb95m}}} (e^{-\lambda_{\text{Nb95m}} t} - e^{-\lambda_{\text{Nb95}} t}) - \frac{\lambda_{\text{Nb95}} A_{\text{Zr95}}^0}{\lambda_{\text{Nb95}} - \lambda_{\text{Zr95}}} (e^{-\lambda_{\text{Zr95}} t} - e^{-\lambda_{\text{Nb95}} t})}{(e^{-\lambda_{\text{Nb95}} t})}$$

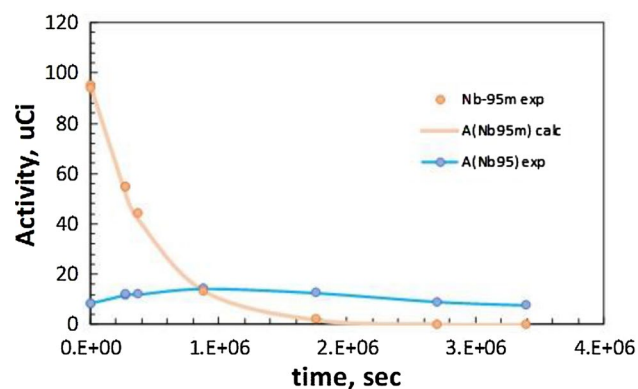


Fig. 4 Ingrowth of ^{95}Nb from decay of $^{95\text{m}}\text{Nb}$

It was experimentally determined that due to the very small production of ^{95}Zr , ingrowth of ^{95}Nb from ^{95}Zr was minimal and could be ignored for simplicity. Ingrowth of ^{95}Nb is shown in Fig. 4. It should be mentioned that presence of activation products ^{54}Mn , ^{51}Cr , and ^{57}Co was only observed in enriched Mo targets (after the decay of ^{99}Mo) and is due to the impurities mentioned earlier. Typical gamma spectra obtained after irradiation of natural UHP and ^{100}Mo enriched Mo targets are shown in Fig. 5.

Results and discussion

Average detected activities at EOB for natural UHP Mo and ^{100}Mo -enriched targets after 0.5 and 4 h irradiations are listed in Tables 3, 4, 5 and 6. Figure 5 compares the gamma spectra of irradiated natural UHP and ^{100}Mo enriched targets. The major peaks identified correspond very well to previous literature data [18, 20]. The data in Fig. 5 illustrate the minimal production of side-reaction products for enriched ^{100}Mo targets. The major side products identified after irradiation of enriched targets are $^{95,96,97,98\text{m}}\text{Nb}$ isotopes and minor production of ^{95}Zr . No presence of $^{95\text{m}}\text{Nb}$ was identified after irradiation of enriched ^{100}Mo targets; however, direct production of ^{95}Nb was confirmed. This indicates that there is no significant production pathway for $^{95\text{m}}\text{Nb}$ from

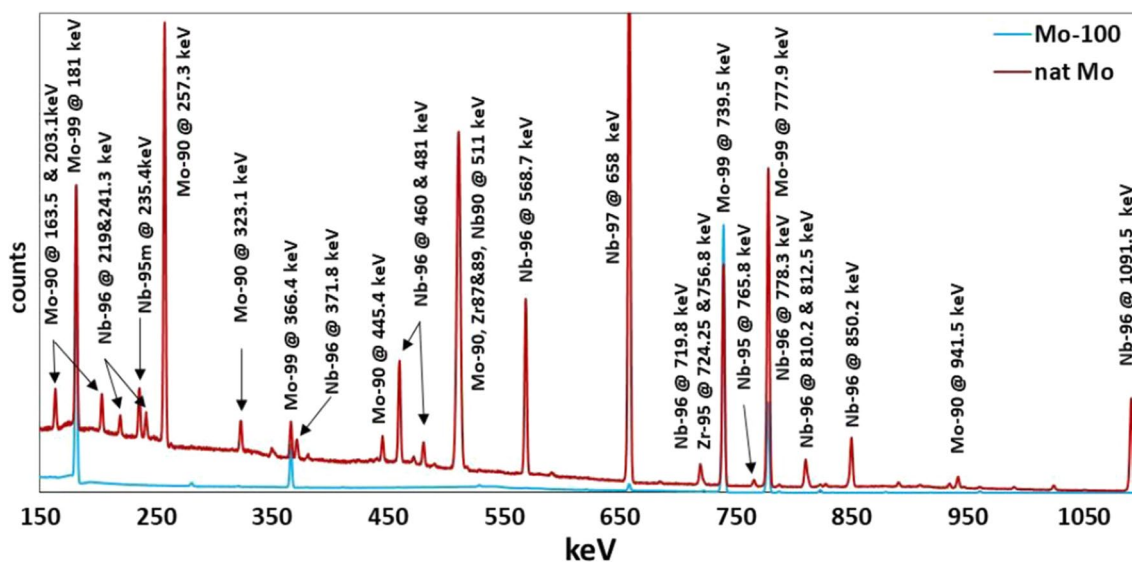


Fig. 5 Gamma spectra of irradiated natural UHP and ^{100}Mo -enriched Mo targets

Table 3 Activities, one-sigma uncertainties, and fraction of activities to that of ^{99}Mo for radioisotopes found in irradiated natural UHP Mo target at EOB. Irradiation: 0.5 h at 40 MeV and 1.5 kW, 0.9736 g Mo target

Radionuclide	A at EOB (μCi)	1σ (%)	$X/^{99}\text{Mo}$ at EOB
^{99}Mo	2.52E+02	3.05%	–
^{90}Mo	7.34E+01	3.08%	29.1%
$^{91\text{m}}\text{Nb}$	N/A	N/A	N/A
$^{92\text{m}}\text{Nb}$	6.52E–01	5.20%	0.259%
$^{95\text{m}}\text{Nb}$	1.41E+01	3.29%	5.61%
^{95}Nb	N/A	N/A	N/A
^{96}Nb	4.26E+01	3.04%	16.9%
^{97}Nb	1.26E+03	3.06%	498.5%
$^{98\text{m}}\text{Nb}$	1.95E+01	8.17%	7.73%
^{88}Zr	N/A	N/A	N/A
^{95}Zr	N/A	N/A	N/A

^{98}Mo , as there is no production on enriched ^{100}Mo target containing ^{98}Mo . Due to the very short half-lives of $^{97,98\text{m}}\text{Nb}$ (Table 2), they are not a concern; however, the production of $^{95,96}\text{Nb}$ (these are produced due to a small content of ^{98}Mo in enriched ^{100}Mo targets) with longer half-lives might be of concern if Nb is not removed from the Mo product, especially if natural Mo targets are used. Their content depends on the level of ^{98}Mo in the target, and for higher enrichments of ^{100}Mo , they should not be a concern. The removal of Zr and Nb isotopes, however, is not difficult, as coprecipitation with Fe(III) is fairly efficient [23]. It also should be noted that production of $^{97\text{m}}\text{Nb}$ was not observed; only direct production of ^{97}Nb was detected.

The analysis of gamma spectra for irradiated enriched ^{100}Mo targets shows the importance of keeping the level of impurities low. As can be seen in Table 6, small levels of ^{51}Cr , ^{54}Mn , and ^{57}Co were detected after irradiation of

Table 4 Activities, one-sigma uncertainties, and fraction of activities to that of ^{99}Mo for radioisotopes found in irradiated natural UHP Mo target at EOB. Irradiation: 4 h at 40 MeV and 1.5 kW, 0.9719 g Mo target

Radionuclide	A at EOB (μCi)	1σ (%)	$X/^{99}\text{Mo}$ at EOB
^{99}Mo	2.00E+03	3.04%	–
^{90}Mo	4.61E+02	4.20%	23.1%
$^{91\text{m}}\text{Nb}$	5.22E+01	3.13%	2.61%
$^{92\text{m}}\text{Nb}$	6.44E+00	3.35%	0.322%
$^{95\text{m}}\text{Nb}$	1.21E+02	3.12%	6.03%
^{95}Nb	7.27E+00	19.15%	0.363%
^{96}Nb	3.30E+02	3.04%	16.5%
^{97}Nb	N/A	N/A	N/A
$^{98\text{m}}\text{Nb}$	N/A	N/A	N/A
^{88}Zr	6.37E–01	3.37%	0.0319%
^{95}Zr	3.17E–02	2.50%	0.00159%

Table 5 Activities, one-sigma uncertainties, and fraction of activities to that of ^{99}Mo for radioisotopes found in irradiated enriched ^{100}Mo (97.39%) target at EOB. Irradiation: 0.5 h at 40 MeV and 1.5 kW, 0.6254 g Mo target

Radionuclide	A at EOB (μCi)	1σ (%)	$X/^{99}\text{Mo}$ at EOB
^{99}Mo	1.49E+03	3.04%	–
^{95}Nb	N/A	N/A	N/A
^{96}Nb	4.71E–01	6.85%	0.0316%
^{97}Nb	1.02E+02	3.29%	6.85%
$^{98\text{m}}\text{Nb}$	1.06E+02	3.33%	7.098%
^{95}Zr	N/A	N/A	N/A
^{51}Cr	N/A	N/A	N/A
^{54}Mn	4.17E–04	8.18%	0.0000280%
^{57}Co	6.57E–04	6.52%	0.0000441%

^{100}Mo -enriched targets; these isotopes are due to the presence of impurities most likely coming from stainless steel. These impurities could have been introduced during target manufacturing or may have been originally present in the enriched Mo material. The source could be linked to equipment, tools, or storage vessels that might be used during enrichment, chemical processing, disk manufacturing, and handling processes. Although the production of these radionuclides is relatively low, if they are not removed, their accumulation in the target might be of concern for recycled targets due to their long half-lives.

For natural Mo targets, the high activity of $^{91\text{m}}\text{Nb}$ ($T_{1/2}=1536.1$ h) at EOB is noticeable (Table 4) and represents $\sim 2.6\%$ of ^{99}Mo activity at EOB. Due to a long half-life, the activity of $^{91\text{m}}\text{Nb}$ remains a significant dose contributor after the decay of ^{99}Mo for long irradiations as well. Sixty days after EOB, when ^{99}Mo activity reaches $\sim 2.7\text{E}-7$ of its original, the activity of $^{91\text{m}}\text{Nb}$ is still at $\sim 50\%$ of its EOB activity. This should be considered a potential source for a high dose when handling waste streams after production of ^{99}Mo using natural targets. $^{91\text{m}}\text{Nb}$ and $^{95\text{m}/95}\text{Nb}$ are the

Table 6 Activities, one-sigma uncertainties, and fraction of activities to that of ^{99}Mo for radioisotopes found in irradiated enriched ^{100}Mo (97.39%) target at EOB. Irradiation: 4 h at 40 MeV and 1.5 kW, 0.4294 g Mo target

Radionuclide	A at EOB (μCi)	1σ (%)	$X/^{99}\text{Mo}$ at EOB
^{99}Mo	9.20E+03	3.04%	–
^{95}Nb	3.15E–02	N/A	0.000343%
^{96}Nb	N/A	N/A	N/A
^{97}Nb	N/A	N/A	N/A
$^{98\text{m}}\text{Nb}$	N/A	N/A	N/A
^{95}Zr	8.18E–02	1.72%	0.000889%
^{51}Cr	1.28E–01	3.19%	0.00139%
^{54}Mn	2.57E–03	3.04%	0.0000279%
^{57}Co	5.75E–03	3.68%	0.0000626%

major side-reaction product contributors to the radiation dose for freshly irradiated natural Mo targets. In contrast to enriched targets, in natural Mo targets production of ^{96}Nb is significant: ~16–17% of ^{99}Mo activity at EOB for a short irradiations. This, however, is not a concern for several-days-long irradiations due to the relatively short half-life of ^{96}Nb ($T_{1/2}=23.35$ h). From other Mo isotopes, only ^{90}Mo was detected in sufficient activities after the short 0.5 h irradiation. No detectable activity of $^{93\text{m}}\text{Mo}$ in irradiated UHP

natural Mo targets was detected by an analysis of gamma peak at 1477 keV, even when gamma counting was performed within an hour after EOB.

Production rates for radioisotopes containing natural UHP Mo and enriched ^{100}Mo identified after 0.5 and 4 h irradiation at 40 MeV are compared with calculated values obtained from the Monte Carlo simulation tool PHITS 3.02 in Tables 7, 8, 9 and 10, and are normalized per mass of Mo target irradiated. This comparison identifies major reaction

Table 7 Comparison of experimental and theoretical production rates for natural UHP molybdenum target at EOB. The 0.9736 g target was irradiated for 0.5 h at 40 MeV and 1.5 kW

Radionuclide	Half-life (h)	Experimental production rate		Theoretical production rate		Comparison rate x (exp)/x(calc)
		1/s/g/kW	x/ ^{99}Mo	1/s/g/kW	x/ ^{99}Mo	
^{99}Mo	66.2	1.22E+09	–	7.94E+08	–	–
^{90}Mo	5.67	3.14E+07	2.57E–02	6.87E+07	8.65E–02	0.296
$^{92\text{m}}\text{Nb}$	243.8	1.16E+07	9.51E–03	4.77E+06	6.01E–03	1.583
$^{95\text{m}}\text{Nb}$	86.6	8.94E+07	7.31E–02	5.57E+06	7.02E–03	10.4
^{95}Nb	839.5	5.78E+07	4.73E–02	5.57E+06	7.02E–03	6.74
^{96}Nb	23.4	7.33E+07	5.99E–02	9.54E+06	1.20E–02	4.99
^{97}Nb	1.23	1.30E+08	1.07E–01	6.37E+06	8.03E–03	13.3
$^{98\text{m}}\text{Nb}$	0.852	1.48E+06	1.21E–03	7.82E+05	9.86E–04	1.23

x/ ^{99}Mo is normalized production rate, x(exp)/x(calc) is ratio of normalized experimental and calculated production rates

Table 8 Comparison of experimental and theoretical production rates for natural UHP molybdenum disks at EOB. The 0.9719 g target was irradiated for 4 h at 40 MeV and 1.5 kW

Radionuclide	Half-life (h)	Experimental production rate		Theoretical production rate		Comparison rate x (exp)/x(calc)
		1/s/g/kW	x/ ^{99}Mo	1/s/g/kW	x/ ^{99}Mo	
^{99}Mo	66.2	1.24E+09	–	7.86E+08	–	–
^{90}Mo	5.67	3.03E+07	2.44E–02	5.53E+07	7.03E–02	0.348
$^{91\text{m}}\text{Nb}$	1536	7.35E+08	5.94E–01	5.72E+08	7.27E–01	0.816
$^{92\text{m}}\text{Nb}$	243.8	1.45E+07	1.17E–02	4.58E+06	5.83E–03	2.00
$^{95\text{m}}\text{Nb}$	86.6	9.74E+07	7.88E–02	5.57E+06	7.09E–03	11.1
^{95}Nb	839.5	5.83E+07	4.71E–02	5.76E+06	7.33E–03	6.42
^{96}Nb	23.4	7.48E+07	6.05E–02	8.72E+06	1.11E–02	5.45
^{88}Zr	2001.7	1.17E+07	9.44E–03	2.31E+06	2.93E–03	3.22
^{95}Zr	1545.6	4.49E+05	3.63E–04	1.39E+05	1.76E–04	2.06

x/ ^{99}Mo is normalized production rate, x(exp)/x(calc) is ratio of normalized experimental and calculated production rates

Table 9 Comparison of experimental and theoretical production rates for enriched ^{100}Mo (97.39%) target at EOB. The 0.6254 g target was irradiated for 0.5 h at 40 MeV and 1.5 kW

Radionuclide	Half-life (h)	Experimental production rate		Theoretical production rate		Comparison rate x (exp)/x(calc)
		1/s/g/kW	x/ ^{99}Mo	1/s/g/kW	x/ ^{99}Mo	
^{99}Mo	66.2	1.13E+10	–	8.13E+09	–	–
^{96}Nb	23.4	1.26E+06	1.12E–04	7.41E+05	9.12E–05	1.23
^{97}Nb	1.23	1.64E+07	1.46E–03	6.17E+06	7.59E–04	1.92
$^{98\text{m}}\text{Nb}$	0.852	1.25E+07	1.11E–03	8.13E+06	1.00E–03	1.11
^{54}Mn	7488	3.55E+05	3.16E–05	6.23E+04	7.66E–06	4.12
^{57}Co	6588	4.93E+05	4.38E–05	3.55E+04	4.36E–06	10.0

x/ ^{99}Mo is normalized production rate, x(exp)/x(calc) is ratio of normalized experimental and calculated production rates

Table 10 Comparison of experimental and theoretical production rates for enriched ^{100}Mo (97.39%) target at EOB. The 0.4294 g target was irradiated for 4 h at 40 MeV and 1.5 kW

Radionuclide	Half-life (h)	Experimental production rate		Theoretical production rate		Comparison x (exp)/x(calc)
		1/s/g/kW	x/ ^{99}Mo	1/s/g/kW	x/ ^{99}Mo	
^{99}Mo	66.2	1.29E+10	–	7.57E+09	–	–
^{95}Nb	839.5	3.66E+05	2.84E–05	7.28E+04	9.62E–06	2.95
^{95}Zr	1545.6	2.78E+06	2.15E–04	5.11E+05	6.75E–05	3.19
^{51}Cr	664.8	1.77E+06	1.37E–04	1.80E+05	2.38E–05	5.76
^{54}Mn	7488	3.99E+05	3.10E–05	6.04E+04	7.98E–06	3.88
^{57}Co	6588	7.85E+05	6.09E–05	4.58E+04	6.05E–06	10.1

x/ ^{99}Mo is normalized production rate, x(exp)/x(calc) is ratio of normalized experimental and calculated production rates

pathways for certain side-reaction products occurring in ^{100}Mo -enriched targets, which in our case contained only ^{98}Mo and ^{100}Mo isotopes. In general, the most likely isotopic contaminant in highly enriched ^{100}Mo material is ^{98}Mo , due to its similar mass; however some presence of lighter Mo isotopes is also possible. Analysis of enriched ^{100}Mo material used in this study showed only the presence of ^{100}Mo (97.39%) and ^{98}Mo (2.59%).

In general, experimentally obtained production rates were higher than those calculated using the Monte Carlo simulation tool PHITS 3.02. Average experimental production rates for ^{99}Mo from irradiating natural Mo targets (1.23E+09–9.63% ^{100}Mo) correlate very well to those obtained after irradiation of ^{100}Mo -enriched targets (1.21E+10–97.39% ^{100}Mo). When production rates for ^{99}Mo are normalized per mass of ^{100}Mo in the target, the average production rate is 1.26E+10 with a standard deviation of 5.7%. This suggest that experimentally obtained data for different lengths of irradiation and content of ^{100}Mo agrees very well with production rates of ^{99}Mo . For enriched targets, relatively good correlation of experimental and calculated production rates was obtained for $^{98\text{m}}\text{Nb}$ and ^{96}Nb . For the rest of the radionuclides, computer models significantly under-predict production rates. It is important to consider this when predicting the purity of the final ^{99}Mo product for enriched ^{100}Mo in a production facility. Because enriched material will be recycled multiple times, those impurities can accumulate in the target material and might require additional chemical purification steps to meet purity requirements.

To determine the production rates of other radionuclides, we looked at irradiated enriched ^{100}Mo targets more closely (Table 11). Because only two Mo isotopes (^{98}Mo and ^{100}Mo) were present in significant quantities in enriched targets, the analysis is a bit easier than that for natural Mo targets.

For ^{95}Nb , there is no production pathway on ^{100}Mo , and therefore any production of ^{95}Nb on an enriched target is due to the presence of ^{98}Mo via $^{98}\text{Mo}(\gamma, 2n + p)^{95}\text{Nb}$. The experimental production rate for this reaction is 1.41E+07 atoms/s/kw/g ^{98}Mo . The contribution of reactions on ^{96}Mo

Table 11 Experimental production rates at 40 MeV for some Nb isotopes normalized per gram of ^{98}Mo

Radionuclide	Target Natural UHP Mo atoms/s/kw/g ^{98}Mo	Target Enriched ^{100}Mo atoms/s/kw/g ^{98}Mo
^{95}Nb	2.41E+08	1.41E+07
^{96}Nb	3.07E+08	4.86E+07
^{97}Nb	5.40E+08	6.34E+08

Table 12 Comparison of normalized production rates for various Nb isotopes

Reaction	Experimental x/ ^{99}Mo PR	Calculated x/ ^{99}Mo PR	Literature [17] x/ ^{99}Mo PR
$^{98}\text{Mo}(\gamma, 2n + p)^{95}\text{Nb}$	1.12E–03	3.46E–04	5.93E–04
$^{98}\text{Mo}(\gamma, p + n)^{96}\text{Nb}$	3.86E–03	3.52E–03	3.15E–03
$^{97}\text{Mo}(\gamma, p)^{96}\text{Nb}$	2.05E–02	1.13E–03	4.51E–03
$^{98}\text{Mo}(\gamma, p)^{97}\text{Nb}$	4.65E–02	2.90E–02	2.58E–03

and ^{97}Mo ($^{96}\text{Mo}(\gamma, p)^{95}\text{Nb}$, $^{97}\text{Mo}(\gamma, p + n)^{95}\text{Nb}$) in natural targets is about 17× higher than that on ^{98}Mo (2.41E+08 vs. 1.41E+07) when normalized per mass of ^{98}Mo .

Similarly, for ^{96}Nb there is no production pathway on ^{100}Mo , and, therefore, any production of ^{96}Nb on enriched targets is via $^{98}\text{Mo}(\gamma, p + n)^{96}\text{Nb}$. For production of ^{96}Nb , it seems that the experimental production rate for the reaction $^{98}\text{Mo}(\gamma, p + n)^{96}\text{Nb}$ is 4.86E+07, and for the $^{97}\text{Mo}(\gamma, p)^{96}\text{Nb}$ reaction it is 2.58E+08 (3.07E+08 minus 4.86E+07). The major reaction pathway for the production of ^{97}Nb is from ^{98}Mo via $^{98}\text{Mo}(\gamma, p)^{97}\text{Nb}$, as the theoretical production rate for reaction on ^{100}Mo is ~1000× lower [17]. The experimental production rate of ^{97}Nb determined after irradiation of the natural Mo target is 5.4E+08 atoms/s/kw/g- ^{98}Mo , and for irradiated enriched ^{100}Mo target is 6.34E+08, giving an average of 5.87E+08 with a standard deviation of 11%.

Experimental production rates for various Nb isotopes are further compared with calculated production rates and

literature data in Table 12. It can be seen that for all these isotopes, experimental production rate ratios or normalized production rates are higher than the calculated and literature data [17].

Considerable production of ^{95}Zr was observed only after 4 h irradiation. If it is assumed that the major reaction pathway for ^{95}Zr in the enriched ^{100}Mo target is due to the presence of ^{98}Mo and the reaction $^{98}\text{Mo}(\gamma, n + 2p)^{95}\text{Zr}$, it would be expected that the total activity of ^{95}Zr produced should be higher using a natural Mo target, due to its higher content of ^{98}Mo (~ 21 × more ^{98}Mo in natural Mo than in enriched ^{100}Mo). However, the opposite was observed, with a higher production of ^{95}Zr in the enriched ^{100}Mo target (Table 13). The content of ^{100}Mo in the irradiated enriched Mo target (0.4294 g Mo) is about 4.5 × higher than in the natural Mo target (0.9719 g of Mo), and the activity of ^{95}Zr produced is ~ 2.7 × higher in the enriched target. Although this doesn't provide excellent correlation to the mass of ^{100}Mo , it does point to a conclusion that major production of ^{95}Zr is due to the reaction on ^{100}Mo via $^{100}\text{Mo}(\gamma, n + \alpha)^{95}\text{Zr}$. However, it should be noted that reactions on $^{97,98}\text{Mo}$ have comparable, but slightly lower, production rates. Table 13 summarizes this discussion. The presence of the Zr impurity in enriched ^{100}Mo material was 50 ppb, so activation of ^{96}Zr is very unlikely, due to a low content of Zr and low natural abundance of ^{96}Zr (2.8%).

The cumulative experimental production rates for natural Mo targets for 0.5 and 4 h irradiations presented in Tables 7 and 8 agree reasonably well for most of the listed radionuclides. The experimental production rate for ^{90}Mo after 0.5 h irradiation is 3.14E+07 and 3.03E+07 after 4 h irradiation. Similarly good correlations can be seen for ^{95}Nb and ^{96}Nb . Differences in experimental production rates obtained for $^{92\text{m}}\text{Nb}$ and $^{95\text{m}}\text{Nb}$ after 0.5 and 4 h irradiation are slightly higher, but reasonable agreement was still observed. It should be noted that these production rates are for all combined reaction pathways listed in Table 2.

Comparison of short-term and long-term duration irradiations

Results of the long irradiation of Mo performed in 2015 were reported previously [24]. In the 2015 irradiation, enriched and natural molybdenum disks were irradiated for a period of 6.5 days. The target was composed of twenty-five Mo disks containing six ^{100}Mo enriched disks (positions

5–10) and nineteen natural Mo disks. A summary of gamma counting results for the natural Mo target from this irradiation run is presented in Table 14.

Total ^{99}Mo activity produced in 6 g of ^{100}Mo enriched target (95.08% ^{100}Mo) was ~ 12.4 Ci. The production of ^{95}Zr and Nb isotopes in the enriched ^{100}Mo target was not quantified, since most of the activity of Zr and Nb was removed after the co-precipitation with Fe followed by filtration [24]. However, the presence of $^{92\text{m}}\text{Nb}$ in the irradiated enriched ^{100}Mo target confirms the presence of lighter Mo isotopes such as ^{94}Mo .

Table 15 compares experimental production rates for short (4 h irradiation at 40 MeV) and long-term (6.5 days at 42 MeV) irradiations normalized per mass of ^{100}Mo . It is important to point out the significant difference between short and long-term irradiation conditions. In short irradiation, we used a high-Z converter (Ta) to produce a hard x-ray spectrum, while in long-term irradiations, a high-Z converter was not used; instead, the conversion process was realized in the actual Mo target. In addition, the energy distribution of the bremsstrahlung photons was different due to the different thickness of the material in the converter. It should also be noted that the target for long-term irradiation was composed of twenty-five Mo disks, and for this comparison, gamma counting data obtained for the disk in position two, close to the converter, was used. Despite the differences in irradiation setup, normalized production rates for most isotopes (except $^{92\text{m}}\text{Nb}$) were quite similar and were within the same order of magnitude. The correlation of the ^{99}Mo

Table 14 Summary of gamma counting results from 6.5 d irradiation of one natural Mo target (position 2 out from 25 disks) irradiated at 42 MeV and 8 kW reported for long-lived radionuclides. Gamma counting of non ^{99}Mo radionuclides was performed after the decay of ^{99}Mo (4 weeks after EOB)

Radionuclide	$T_{1/2}$ (h)	42 MeV experimental $X^{99}\text{Mo}$	EOB mCi/1 Ci ^{99}Mo	60d after EOB, mCi
$^{91\text{m}}\text{Nb}$	1536.12	6.10%	61	31.8
$^{92\text{m}}\text{Nb}$	243.84	0.89%	8.9	0.148
$^{95\text{m}}\text{Nb}$	85.6	8.66%	86.6	0.001
^{95}Nb	839.5	1.60%	16.0	7.906
^{88}Zr	2001.6	0.077%	0.770	0.468
^{95}Zr	1536.5	0.0030%	0.030	0.016
^{99}Mo	66.2	100%	1000	0.27

Table 13 Comparison of ^{95}Zr production on natural and enriched ^{100}Mo targets for 4 h irradiation at 40 MeV

Mo target	Production rate				
	^{95}Zr , μCi at EOB	^{98}Mo (g)	^{100}Mo (g)	1/s/g $^{100}\text{Mo}/\text{kW}$	1/s/g $^{98}\text{Mo}/\text{kW}$
UHP	0.032	0.235	0.094	4.66E+06	1.86E+06
Enriched ^{100}Mo	0.087	0.011	0.418	2.85E+06	8.50E+08

Table 15 Comparison of experimental production rates calculated from 6.5 d irradiation of the natural target and results from short 4 h irradiations, normalized per mass of ^{100}Mo

Radionuclide	Short irradiation (4 h) atoms/s/kw/g ^{100}Mo	Long irradiation (6.5d) atoms/s/kw/g ^{100}Mo	Production rate ratios, X-short/X- long
^{99}Mo	1.26E+10	1.26E+10	–
$^{91\text{m}}\text{Nb}$	6.56E+09	9.22E+09	0.712
$^{92\text{m}}\text{Nb}$	1.21E+08	2.55E+08	0.475
$^{95\text{m}}\text{Nb}$	1.01E+09	1.23E+09	0.731
^{95}Zr	4.66E+06	4.55E+06	1.024

and ^{95}Zr production rates for short (4 h) and long (6.5 d) irradiations is very good. Such a great agreement for ^{99}Mo production is probably coincidental given the dramatic difference in irradiation conditions; however, the production of ^{95}Zr is good example of the agreement of experimentally determined production rates.

Conclusions

Irradiations of a natural UHP Mo and an enriched ^{100}Mo target at 40 MeV were performed to obtain basic information about the identification of major side-reaction products. Experimental results were compared to computer simulations using Monte Carlo simulation code PHITS 3.02, and the experimental results obtained from 4 h irradiations at 40 MeV were compared to previously obtained results from 6.5 d irradiations at 42 MeV. A very good correlation for ^{99}Mo experimental production rates was observed for 0.5 h, 4 h, and 6.5 d irradiations. It was determined that production of ^{95}Nb and ^{96}Nb is associated with the presence of ^{98}Mo in enriched ^{100}Mo , and there is no appreciable production rate on natural ^{100}Mo . Moreover, the major production pathway for production of ^{97}Nb in enriched ^{100}Mo is due to the presence of ^{98}Mo .

Calculated production rates are largely in close agreement with experimentally obtained ^{99}Mo production rates, but, except for ^{90}Mo , the computer model significantly under-predicts the production rates of other radioisotopes. It is important to take this into account when predicting the purity of the final ^{99}Mo product for enriched ^{100}Mo . This was especially true of the calculated production rates for ^{51}Cr , ^{54}Mn , and ^{57}Co (due to the presence of Cr, Mn, and Ni impurities in the enriched ^{100}Mo target), which were more than a $3 \times$ lower than those determined experimentally. This is particularly important to tracking the impurity level in the original enriched material as well as to the introduction of elements during the recycling of enriched material, due to long half-lives and a potential build-up of activity. Because enriched material will be recycled multiple times, those impurities can accumulate in the target material and

might require additional chemical purification steps to meet purity specifications.

Acknowledgements Work supported by the U.S. Department of Energy, NNSA's Material Management and Minimization office, under Contract DE-AC02-06CH11357. Argonne National Laboratory is operated for the U.S. Department of Energy by UChicago Argonne, LLC.

References

- National Research Council (2009) Medical isotope production without highly enriched uranium. The National Academies Press, Washington, DC. <https://doi.org/10.17226/12569>
- Morley T, Gagnon K, Schaffer P, Asselin E, Zeisler S (2011) Cyclotron production of technetium. *J Nucl Med* 52:291
- Benard F, Buckley KR, Ruth TJ, Zeisler SK, Klug J, Hanemaayer V, Vuckovic M, Hou X, Celler A, Appiah JP, Valliant J, Kovacs MS, Schaffer P (2014) Implementation of multi-curie production of Tc-99m by conventional medical cyclotrons. *J Nucl Med* 55:1017–1022
- Eslami M, Kakavand T (2014) Simulation of the direct production of Tc-99m at a small cyclotron. *Nucl Instrum Methods Phys Res B* 329:18–21
- Dick D (2014) Diversification of Mo-99/Tc-99m supply. *J Nucl Med* 55:875–876
- Manenti S, Holzwarth U, Loriggiola M, Gini L, Esposito J, Groppi F, Simonelli F (2014) The excitation functions of Mo-100(p, x)Mo-99 and Mo-100(p,2n)Tc-99m. *Appl Radiat Isotopes* 94:344–3448
- Bennett RG, Christian JD, Petti DA, Terry WK, Grover SB (1998) A system of $^{99\text{m}}\text{Tc}$ production based on distributed electron accelerators and thermal separation. *Nucl Technol* 126:102–121
- Sabel'nikov A, Maslov O, Molokanova L, Gustova M, Dmitriev S (2006) Preparation of ^{99}Mo and $^{99\text{m}}\text{Tc}$ by $^{100}\text{Mo}(\gamma, n)$ photo-nuclear reaction on an electron accelerator, MT- 25 microtron. *Radiochemistry* 48:191–194
- Starovoitova V, Tchelidze L, Wells D (2014) Production of medical radioisotopes with linear accelerators. *Appl Radiat Isotopes* 85:39–44
- Dale G, Chemerisov S, Vandegrift G, Tkac P, Woloshun K, Bach H, Heath C, Kelsey C, Bowers D, Gelis AV, Jonah C, McCrady R, Olivas E, Hurtle K, Pitcher E, Romero F, Tuzel W, Giola J, Tomei T, Wheat R, DeCroix M, Warren D, Dalmas D, Romero B, Harvey JT (2010) Global threat reduction initiative (GTRI) accelerator production of ^{99}Mo . Los Alamos National Laboratory, LA-UR-11-, 2010 Report
- Gagnon K, Wilson JS, Holt CMB, Abrams DN, McEwan AJB, Mitlin D, McQuarrie SA (2012) Cyclotron production of $^{99\text{m}}\text{Tc}$:

- recycling of enriched ^{100}Mo metal targets. *Appl Radiat Isotopes* 70:1685–1690
12. Tkac P, Vandegrift GF (2015) Recycle of enriched Mo targets for economic production of $^{99}\text{Mo}/^{99\text{m}}\text{Tc}$ medical isotope without use of enriched uranium. *J Radioanal Nucl Chem* 308:205–212
 13. Tkac P, Momen A, Wardle K, Copple JM, Brown MA, Vandegrift GF (2017) MOEX: Solvent extraction approach for recycling enriched $^{98}\text{Mo}/^{100}\text{Mo}$ material. *Sep Sci Technol* 53:1856–1863
 14. Kozak PA, Tkac P, Wardle KE, Brown MA, Vandegrift GF (2020) Demonstration of the MOEX Process Using Additive-Manufacturing-Fabricated Annular Centrifugal Contactors. *Solvent Extr Ion Exchange* 38:120–131
 15. Food US and Drug Administration (FDA) (2018). FDA and NRC pave way for the first domestic supply of the most commonly used medical isotope in diagnostic imaging, news release. www.fda.gov/NewsEvents/Newsroom/PressAnnouncements/ucm595990.htm
 16. Beil H, Bergere R, Carlos P, Lepretre A, De Miniac A, Veysiere A (1974) A study of the photoneutron contribution to the giant dipole resonance in doubly even Mo isotopes. *Nucl Phys A* 227:427–449
 17. Martin T, Harahsheh T, Munoz B, Hamoui Z, Clanton R, Douglas J, Brown P, Akabani G (2017) Production of $^{99}\text{Mo}/^{99\text{m}}\text{Tc}$ via photoneutron reaction using natural molybdenum and enriched ^{100}Mo : part 1, theoretical analysis. *J Radioanal Nucl Chem* 314:1051–1062
 18. Ishkhanov BS, Kapitonov IM, Kuznetsov AA, Orlin VN (2014) Photodisintegration of molybdenum isotopes. *Mosc U Phys B+* 69:37–46
 19. Kelsey CT, Chemerisov SD, Dale GE, Harvey J, Tkac P, Vandegrift GF (2011) MCNPX-CINDER'90 simulation of photonuclear Mo-99 production experiments. Los Alamos National Laboratory LA-UR-11-10487
 20. Takeda T, Fujiwara M, Kurosawa M, Takahashi N, Tamura M, Kawabata T, Fujikawa Y, Suzuki KN, Abe N, Kubota T, Takahashi T (2018) $^{99\text{m}}\text{Tc}$ production via the (γ, n) reaction on natural Mo. *J Radioanal Nucl Chem* 318:811–821
 21. Inagaki M, Sekimoto S, Tadokoro T, Ueno Y, Kani Y, Ohtsuki T (2020) Production of $^{99}\text{Mo}/^{99\text{m}}\text{Tc}$ by photonuclear reaction using a natMoO₃ target. *J Radioanal Nucl Chem* 324:681–686
 22. Alford K, Chemerisov S, Gromov R, Hafenrichter L, Jonah CD, Tafoya R, Wesolowski K, Brown D, Forknall S, Gardner J, Macrillo D, Zulpo A (2015) Low energy accelerator facility upgrade and test. In: Proceedings of 12th international topical meeting on the nuclear application of accelerators, Washington D.C
 23. Tkac P, Rotsch D, Stepinski D, Makarashvili V, Vandegrift GF (2015) Optimization of the processing of Mo disks. Argonne National Laboratory, ANL/NE-15/46
 24. Chemerisov S, Bailey J, Heltemes T, Jonah C, Gromov R, Makarashvili V, Tkac P, Rotsch D, Virgo M, Vandegrift GF (2016) Results of the six-and-a-half day electron-accelerator irradiation of enriched Mo-100 targets for the production of Mo-99. Argonne National Laboratory DOI10.2172/1342168

Publisher's Note Springer Nature remains neutral with regard to jurisdictional claims in published maps and institutional affiliations.